Journal of Power Sources 185 (2008) 401–410

Contents lists available at ScienceDirect

Journal of Power Sources

journal homepage: www.elsevier.com/locate/jpowsour

Reactivity between La(Sr)FeO_3 cathode, doped CeO_2 interlayer and yttria-stabilized zirconia electrolyte for solid oxide fuel cell applications

Ana Martínez-Amesti[a], Aitor Larrañaga[a,*], Lide M. Rodríguez-Martínez[b], Andrés T. Aguayo[a], Jose L. Pizarro[a], Maria L. Nó[a], Ander Laresgoiti[b], Maria I. Arriortua[a]

[a] University of the Basque Country (UPV/EHU), Faculty of Science and Technology, B. Sarriena S/N, 48940 Leioa, Vizcaya, Spain
[b] Ikerlan-Energía, Centro Tecnológico, Parque Tecnológico de Alava, Juan de la Cierva 1, 01510 Miñano, Spain

ARTICLE INFO

Article history:
Received 14 February 2008
Received in revised form 21 May 2008
Accepted 8 June 2008
Available online 26 June 2008

Keywords:
SOFC
Reactivity
Interlayer
Doped ceria
Lanthanum ferrite

ABSTRACT

Detailed X-ray diffraction (XRD) analysis of two different Sr-doped $LaFeO_3$ cathodes, YSZ electrolyte and two Sm/Gd-doped CeO_2 interlayer and their mixtures were used to evaluate the formation of undesired secondary reaction compounds. The analysis of room temperature X-ray diffraction data of the mixtures indicates the crystallization of strontium and/or lanthanum zirconates between the cathode and the electrolyte materials and no detected reaction between the cathode and the interlayer materials.

For all the ferrite mixtures a significant shift in the diffraction peaks is observed, which is the result of the unit cell volume expansion and contraction of the cathode (LSF) structures mixed with electrolyte (YSZ), and with interlayers (SDC, GDC), respectively. On the other hand, a complete solid solution was observed between the crystal structures of YSZ electrolyte and SDC or GDC interlayers.

The observed cell modifications for the ferrite mixtures were the result of the incorporation of Zr and Ce, in the B and A type positions of the perovskite structure, respectively. The electrolyte/interlayer interface shows the presence of intermediate compositions at high temperature.

The electrochemical studies show better results when a Sm-doped CeO_2 is inserted between the cathode and electrolyte material. The best result obtained is for the half-cell prepared with LSF-40 and SDC interlayer on YSZ electrolyte.

1. Introduction

Solid oxide fuel cells (SOFC) are electrochemical devices that directly convert chemical energy, through an electrochemical reaction between a fuel and an oxidant, into electrical energy. The basic elements of the typical fuel cell consist of an electrolyte phase in intimate contact with a porous anode and cathode.

SOFCs have exceptional potential as electric power generation systems, because of their high-energy conversion efficiency, which can reach up to 65%. In addition, SOFCs have many advantages such as multi-fuel capability or the simplicity of the system design. Actually, reasonably high power densities and long-term stability have been achieved for high temperature SOFC single cells using La(Sr)FeO_3 (LSF) as cathode and yttria-stabilized zirconia (YSZ) as electrolyte [1].

Some studies show an improved performance of the power densities with the incorporation of a Sm or Gd-doped CeO_2 layer between the Sr-doped lanthanum ferrite cathode and YSZ electrolyte [2].

One potential reason for this development is the enhanced oxygen surface exchange kinetics of ceria compared to zirconia [1] and another is that for LSF perovskites, the ceria acts as a reaction barrier, preventing the formation of poorly conducting phases ($SrZrO_3$, $SrFe_{12}O_{19}$, and $La_2Zr_2O_7$) [3].

Preliminary studies show that the inclusion of Sm or Gd-doped CeO_2 (SDC, GDC) interlayer prevents the formation of strontium and lanthanum phases [4,5]. However, closer examination of the X-ray diffraction (XRD) data for the reacted LSF–(SDC/GDC)–YSZ mixtures revealed different small shift in the LSF peak positions, corresponding to an increase of LSF–YSZ or a decrease of LSF–(SDC/GDC) in the

* Corresponding author at: University of the Basque Country (UPV/EHU), Faculty of Science and Technology, Department of Mineralogy and Petrology, B. Sarriena S/N, 48940 Leioa, Vizcaya, Spain. Tel.: +34 946012599; fax: +34 946013500.
E-mail address: aitor.larranaga@ehu.es (A. Larrañaga).

0378-7753/$ – see front matter © 2008 Elsevier B.V. All rights reserved.
doi:10.1016/j.jpowsour.2008.06.049

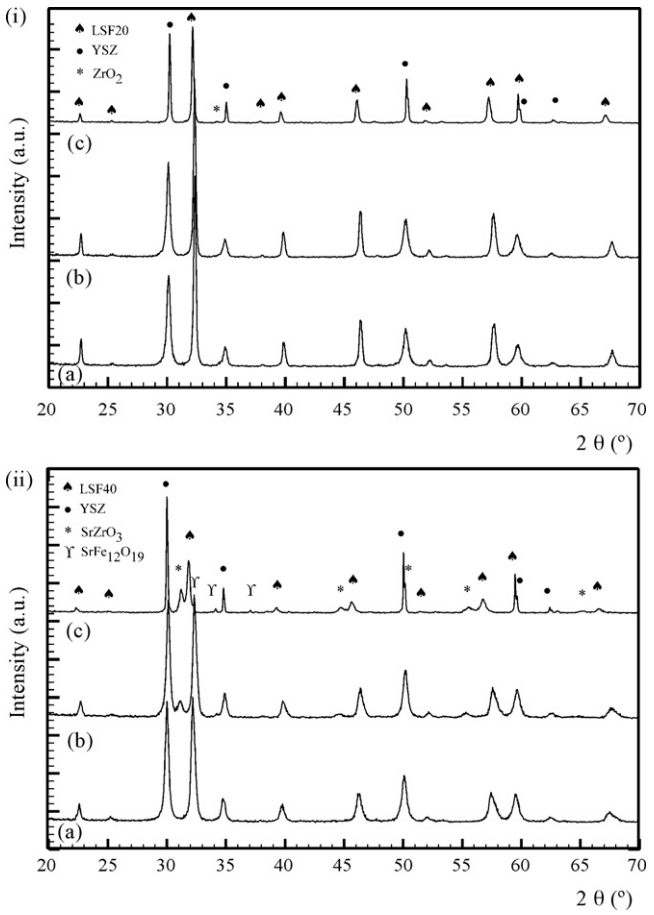

Fig. 1. Room temperature X-ray powder diffraction patterns of $La_{1-x}Sr_xFeO_3$ and YSZ mixtures prepared at (a) 25 °C, (b) 850 °C and (c) 1150 °C. (i) (LSF-20)–YSZ and (ii) (LSF-40)–YSZ.

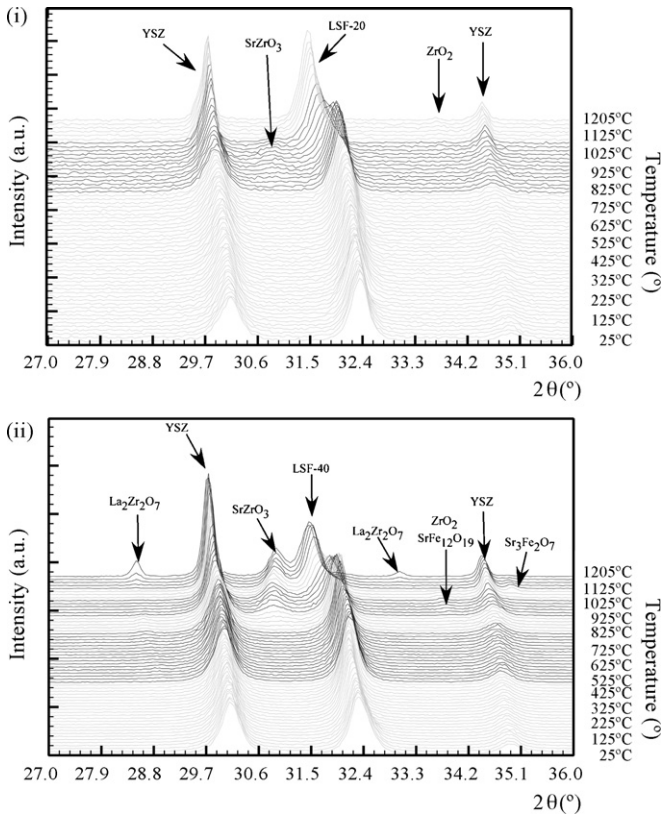

Fig. 2. X-ray thermodiffractograms for (i) (LSF-20)–YSZ and (ii) (LSF-40)–YSZ mixtures.

unit cell volume of these compounds. The ceria-based interlayer also affects the electrolyte interface, giving rise to the formation of intermediate phases.

The aim of this work is to examine the solid-state reaction and interdiffusion phenomena between YSZ electrolyte, doped ceria interlayer and LSF cathode, studied by X-ray diffraction, scanning electron microscopy (SEM) and electrochemical impedance.

2. Experimental

The material powders used in this study were: YSZ powder manufactured from Tosoh Corporation, Sm and Gd-doped CeO_2 ($Ce_{0.8}Gd_{0.2}O_{1.9}$ (GDC), $Ce_{0.8}Sm_{0.2}O_{1.9}$ (SDC)) and $La_{0.8}Sr_{0.2}FeO_3$ (LSF-20) from Praxair Surface Technologies and $La_{0.6}Sr_{0.4}FeO_3$ (LSF-40) from NexTech, Fuel Cell Materials. The selected materials were mixed at 50/50% weight ratio. To assure homogeneity, 10 g of each sample were mixed with 220 g of zirconium 2 mm spheres and 25 ml of acetone in a 100 cm^3 vessel, using an Attritor 01-HD mill. The samples were stirred at 500 rpm for 30 min and then the solvent was evaporated. Powders were then pressed into pellets at 6 tons. The (LSF-20, LSF-40 cathodes + YSZ electrolyte) and (LSF-20, LSF-40 cathodes + SDC, GDC interlayer) mixtures were heated at two different temperatures, 850 and 1150 °C for 2 h at 1 °C min^{-1} heating speed. The different temperatures used to promote the reactions for the (YSZ electrolyte + SDC, GDC interlayers) pellets were 950, 1100, 1200 and 1300 °C for 2 h using 1 °C min^{-1} heating rate.

The room temperature X-ray powder patterns were collected in air on a PHILIPS X'PERT automatic diffractometer operating at 40 kV and 40 mA with Cu Kα radiation. The patterns were recorded in 2θ steps of 0.02° in the 15–80° range, counting for 8 s per step. The thermodiffractometric study was carried out with a PHILIPS X'PERT diffractometer equipped with a variable-temperature stage (Paar Physica TCU2000) with a Pt sample holder. The powder patterns were recorded in 2θ steps of 0.02° in the $15 \leq 2\theta \leq 80$ range, counting for 1 s per step and increasing the temperature at 5 °C min^{-1} from room temperature up to 1205 °C. The powder diffraction data

Table 1
Proportion of secondary phases calculated by X-ray full-profile refinement in cycle mode at different ranges for (LSF-20)–YSZ mixture and (LSF-40)–YSZ mixture

Temperature range (°C)	Secondary phases	wt.% range with the temperature
LSF-20–YSZ		
25–825	None	–
845–1045–1105	$SrZrO_3$	0.2(1)–3.1(2)–0.6(3)
1125–1205	ZrO_2	0.5(1)–0.9(2)
LSF-40–YSZ		
25–525	None	–
545–845	ZrO_2	1.1(1)–1.1(1)
865–925	ZrO_2	2.1(1)–1.7(1)
	$SrZrO_3$	2.0(1)–8.7(2)
945–1065–1125	ZrO_2	0.8(1)–1.5(1)–2.4(2)
	$SrZrO_3$	8.4(2)–16.9(2)–21.0(4)
	$SrFe_{12}O_{19}$	1.1(1)–2.3(1)–0.2(2)
1145–1205	ZrO_2	1.4(1)–0.7(0)
	$SrZrO_3$	16.8(3)–20.7(4)
	$Sr_3Fe_2O_7$	2.0(2)–1.4(1)
	$La_2Zr_2O_7$	0.5(0)–4.2(1)

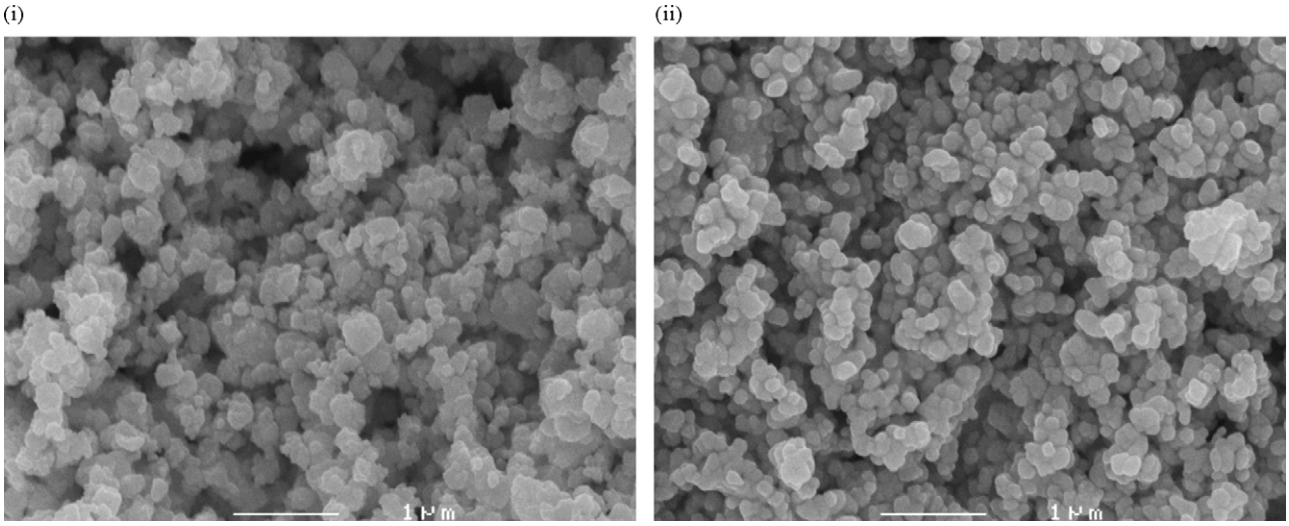

Fig. 3. SEM photographs of (i) LSF-20 and (ii) LSF-40 powders.

of the samples were fitted in all the cases by Rietveld method using the FullProf program [6–8].

The electrochemical half-cells were prepared in the symmetrical configuration with a reference electrode placed more than 5L times the distance from the working electrode and with 0.25 cm^2 area. Both sides of the electrolyte were rectified with manual spraying a Sm-doped CeO_2 (SDC) and Sr-doped lanthanum ferrite (LSF-40, LSF-20) cathode layer. Afterwards these assemblies were heated at 1100 °C for 2 h and 950 °C for 2 h, respectively in air to increase the adherence between the electrodes and electrolyte. The heating–cooling rate during all the treatment was 1 °C min^{-1}. The electronic contact was made using platinum wire and platinum paste. The last one was painted on both sides of the samples as reference electrode and heated at 950 °C in air for 30 min. The electrolyte (YSZ) conductivity was measured using four-probe point configuration. The electronic contact was made using platinum wire and gold paste.

The particle size of LSF perovskites was analyzed by laser dispersion analyzer "Malvern MasterSizerX" and SEM was carried out by using a JEOL JSM-6400 instrument. Brunauer–Emmetty–Teller (BET) [9] surface areas were determined by nitrogen adsorption–desorption in a MICROMERITICS ASAP 2010. AC impedance spectroscopy measurements were carried out using a Solartron 1260 Frequency Response Analyzer coupled to a Solartron 1286 Electrochemical Interface, with voltage amplitude of 60 mV over a frequency range of 1 Hz to 1 MHz.

Table 2
Average particle size calculated by laser dispersion analysis (d_{50}), scanning electron microscopy (d_{SEM}) and specific surface area values (SSA_{BET}) associated

Perovskite	d_{50} (μm)	d_{SEM} (μm)	SSA_{BET} ($m^2\ g^{-1}$)
LSF-20	0.70	0.58	5.85
LSF-40	0.24	0.28	13.30

3. Results and discussion

3.1. Study of the compatibility between the LSF-20/LSF-40 cathodes and YSZ electrolyte

All the X-ray powder diffraction patterns were refined by the Rietveld method. The full-profile refinement of the mixtures were performed starting from the atomic coordinates of each phase [10–16] taken from Inorganic Crystal Structure Database (ICSD)

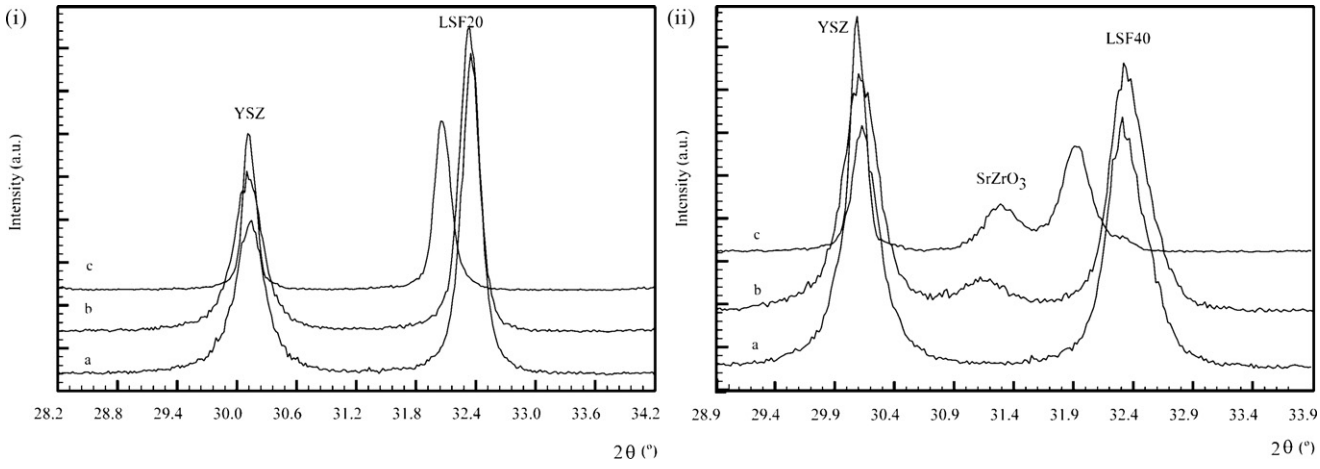

Fig. 4. Slight shift in the LSF peaks observed by X-ray diffraction annealed in the mixtures at (a) 25 °C, (b) 850 °C and (c) 1150 °C for (i) LSF-20–YSZ and (ii) LSF-40–YSZ mixtures.

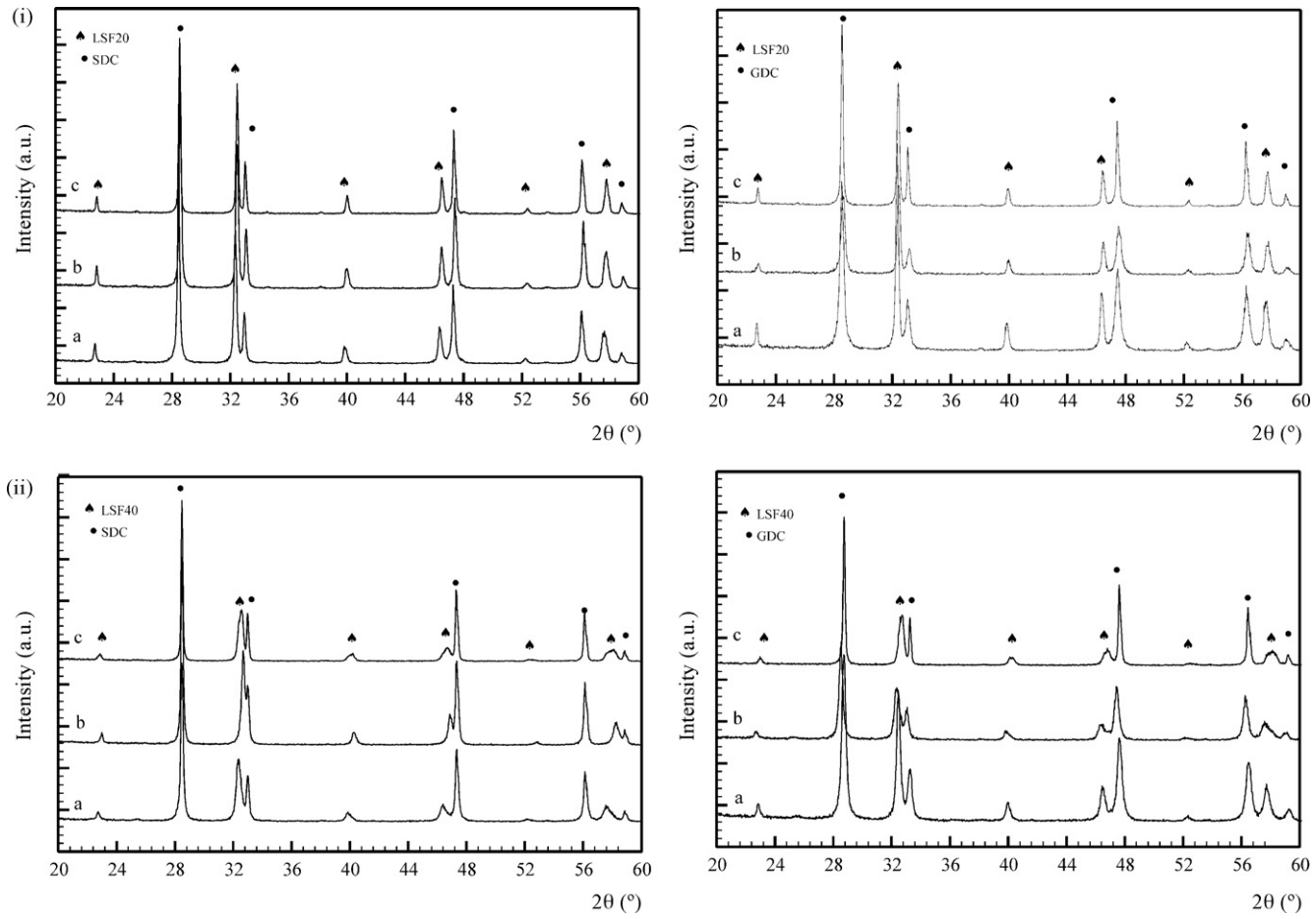

Fig. 5. Room temperature X-ray diffraction patterns for reacted mixtures at different temperatures (a) 25 °C, (b) 850 °C and (c) 1150 °C of (i) LSF-20 and doped ceria compounds and (ii) LSF-40 and doped ceria compounds.

[17], in order to find out the exact proportion of each compound and to guarantee the absence of other compounds with overlapped maxima.

Fig. 1 shows the room temperature X-ray powder patterns of the mixtures treated at three temperatures 25, 850 and 1150 °C. In both cases the LSF–YSZ mixtures show the formation of additional phases (ZrO_2, $SrZrO_3$ and/or $SrFe_{12}O_{19}$). The higher content of strontium in the LSF-40 ferrite promotes the reaction between the mixture's components [18], giving rise to the formation of strontium phases as $SrZrO_3$ and/or $SrFe_{12}O_{19}$ consistent to the amount of this element in the original LSF-40 perovskites, whereas, with LSF-20 only ZrO_2 appeared at high temperatures.

Thermodiffractometric study (TDX) (Fig. 2) was carried out in order to evaluate the weight proportion and thermal stability of the secondary phases (Table 1).

The higher reactivity of LSF-40 is related with the higher strontium content, but also with the smaller particle size and the higher surface area compared to LSF-20 used in this study. Fig. 3 shows SEM images of LSF-20 and LSF-40 powders representing that LSF-40 powder was composed by less aggregated particles. Table 2 shows the average particle size calculated by laser dispersion analysis and SEM with the corresponding specific surface area obtained by BET measurement for both samples.

Closer examination of the LSF–YSZ room temperature X-ray diffraction patterns of the samples treated at high temperatures, reveal a slight shift to lower angle in the LSF peaks (Fig. 4), which corresponds to an increase of the unit cell parameters. The unit cell volume values of YSZ remains constant in the complete temperature range, however the ferrites show in both cases a unit cell expansion at 1150 °C of 2.51 and 4.15% for LSF-20 and LSF-40, respectively.

As was indicated in previous works (see Ref. [3]), a replacement of Y or Zr cations in the B position of the perovskite structure would result in a unit cell expansion (observed in the studied sample) due to their ionic radii [18] (Y^{3+} 0.9 Å and Zr^{4+} 0.72 Å) increased in comparison to any of the Fe cations (0.55–0.78 Å) present in the ferrite.

3.2. Study of the compatibility of LSF-20/LSF-40 with SDC/GDC materials

X-ray diffraction patterns for the LSF/Sm or Gd-doped ceria mixtures treated at room temperature, 850 and 1150 °C are shown in Fig. 5. The X-ray diffraction analyses do not reveal additional secondary reaction phases; however, a slight shift to higher angle can be observed for the ferrite peaks. This effect was analyzed using X-ray powder diffraction full-profile refinement by the Rietveld method. The refinement allows quantification of the displacement of the peaks, in order to calculate the decrease of the unit cell volume. In the four cases, the ferrites show a decrease of the unit cell volume of 0.22, 0.19, 1.06 and 1.45% for LSF-20 mixed with SDC and GDC, and for LSF-40 mixed with SDC and GDC, respectively in the samples treated at 1150 °C.

The observed decrease of the volume was in good agreement with a partial substitution of La and/or Sr in the ferrites by Ce and/or Sm and/or Gd of the interlayer. These elements have similar atomic

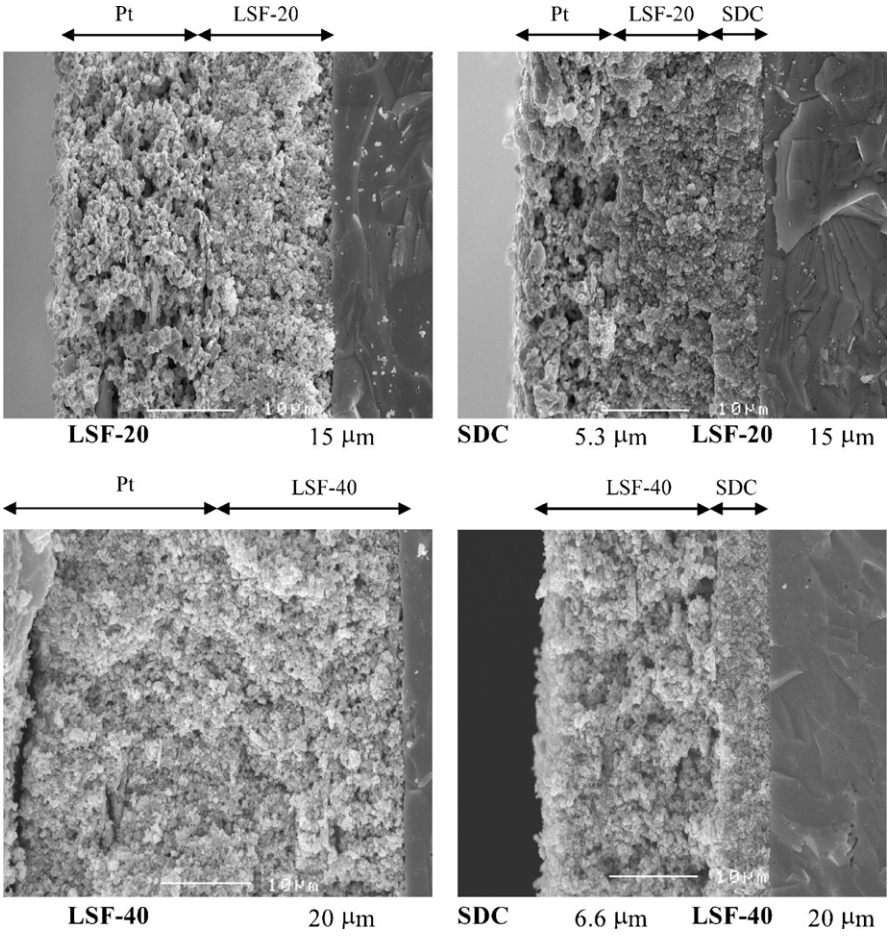

Fig. 6. SEM micrograph of the cross-section for prepared cells with (right) and without (left) interlayer.

radii (Ce^{4+} 0.87 Å; Sm^{3+} 0.96 Å; Gd^{3+} 0.94 Å; La^{3+} 1.36 Å; Sr^{2+} 1.44 Å) [18], therefore, the replacement was possible and as the replaced atoms were bigger than the ones that were incorporated in the ferrites, the unit cell volume was reduced.

3.3. Electrochemical study of both systems (with or without interlayer)

Electrochemical measurements were performed using three electrode cell configurations. The influence of the ceria interlayer was studied by measuring half-cells with and without interlayer at different current densities (0–300 mA) and temperatures (700 and 800 °C) by impedance spectroscopy.

The electrolyte ionic conductivity measurement was made. The resistivity values obtained for this measurement at 800 and 700 °C were 20.05 and 59.57 Ω cm, respectively. The ohmic resistances shown in Table 3 are in good agreement with the expected values calculated taking into account the electrolyte thickness and measured resistivity. The ohmic resistances are in 0.25–0.52 Ω cm^2 range, due to the electrolyte thickness variability.

Fig. 6 shows a scanning electron micrograph of the half-cells cross-section, for samples with and without the SDC interlayer. As can been seen, the electrode and/or interlayer adheres well on the electrolyte under the process conditions used to fabricate the cell. The cathode and interlayer thickness determined from SEM observations were in the 15–20 and 5–7 μm range, respectively, for all the samples.

The EIS studies at OCP conditions and under polarization at 100 and 300 mA are shown in Fig. 7 at 700 and 800 °C. In general, it is observed that the incorporation of the (Sm doped) CeO_2 layer decreases the electrochemical resistance of the system (Table 3). The best results correspond to the half-cell with SDC interlayer and LSF-40 as cathode material.

The change in performance by the presence of the SDC layer is more pronounced for the LSF-40 cathode than for LSF-20. This may evidence the role of the interlayer preventing chemical reaction between cathode and electrolyte. There is still an improvement in the performance, associated with the presence of the interlayer, probably due to the better oxygen surface exchange kinetics of ceria compared to zirconia and the role of the interlayer as reaction barrier, preventing the formation of poorly conducting new phases. In addition, the decrease of the unit cell volume of the ferrites, which is a consequence of the partial substitution of La and/or Sr in the perovskites by Ce and/or Sm from the interlayer, should improve the ionic conductivity of the cathode.

3.4. Compatibility between YSZ electrolyte and doped ceria interlayer (SDC, GDC)

In order to understand the exact role of the ceria-based interlayer, it is necessary to study the thermal stability and the compatibility between the electrolyte (YSZ) and interlayer (SDC, GDC) compounds.

The prepared mixtures have been studied by X-ray powder diffraction and refined using the full-profile refinement by Full-

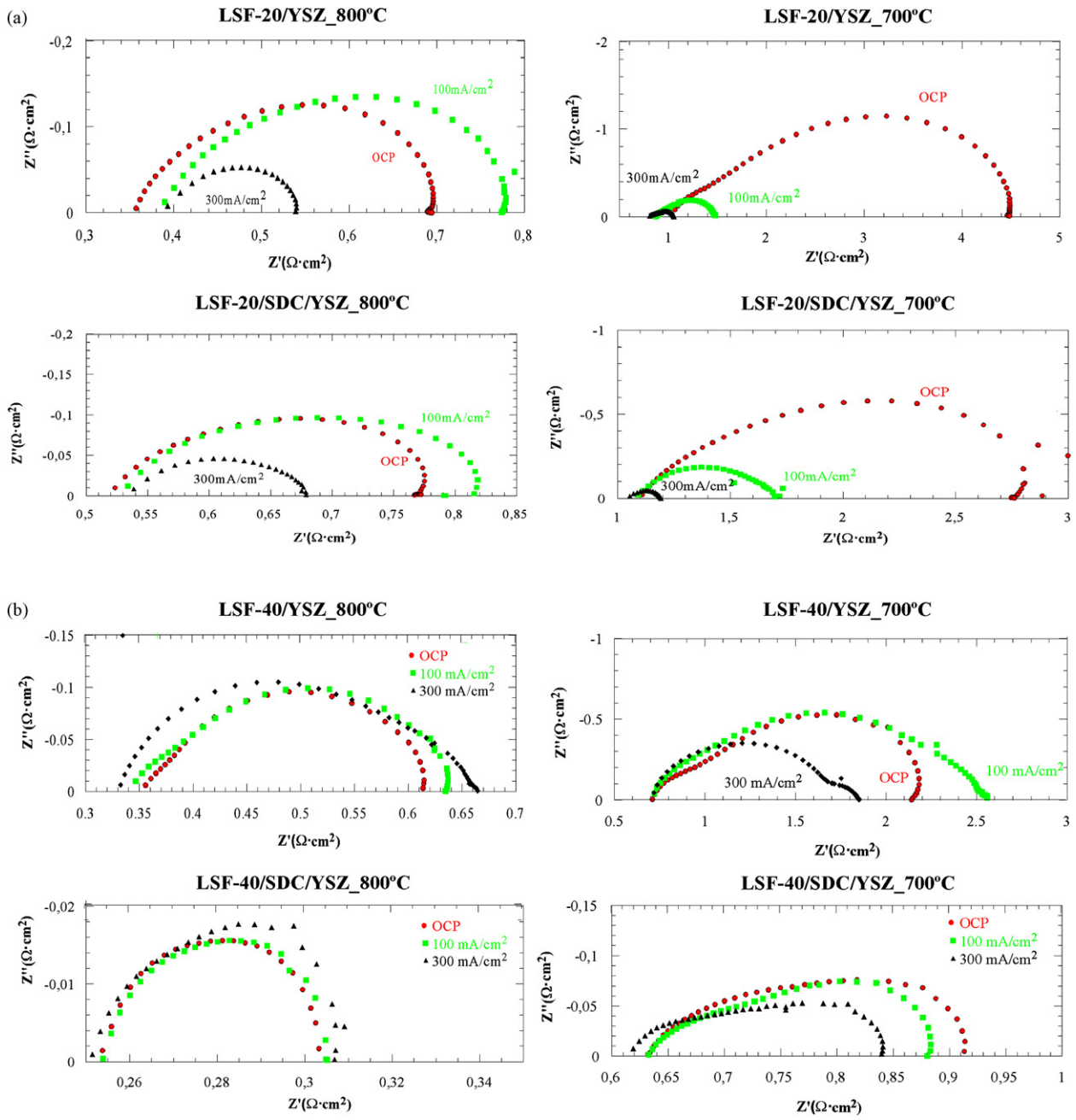

Fig. 7. Impedance diagrams for electrode/electrolyte and electrode/interlayer/electrolyte half-cells at 800 and 700 °C for (a) LSF-20 and (b) LSF-40 cathodes measured at OCP, 100 and 300 mA.

Table 3
Ohmic resistance (R_Ω), area specific resistance (ASR) and polarization resistance (R_p) obtained by impedance spectroscopy (OCP, 100 and 300 mA)

T	Cell	R_Ω (Ω cm^2)			ASR (Ω cm^2)			R_p (Ω cm^2)		
		OCP	100 mA	300 mA	OCP	100 mA	300 mA	OCP	100 mA	300 mA
800 °C	LSF-20/YSZ	0.35	0.38	0.38	0.69	0.77	0.54	0.34	0.39	0.16
	LSF-20/SDC/YSZ	0.52	0.52	0.54	0.77	0.81	0.68	0.25	0.29	0.14
	LSF-40/YSZ	0.35	0.34	0.33	0.61	0.63	0.66	0.26	0.29	0.33
	LSF-40/SDC/YSZ	0.25	0.30	0.25	0.30	0.30	0.31	0.05	0.05	0.05
700 °C	LSF-20/YSZ	1.01	0.86	0.80	4.46	1.48	1.05	3.45	0.61	0.25
	LSF-20/SDC/YSZ	1.11	1.07	1.04	2.45	1.73	1.20	1.34	0.66	0.16
	LSF-40/YSZ	0.71	0.71	0.71	2.13	2.53	1.85	1.42	1.82	1.14
	LSF-40/SDC/YSZ	0.63	0.63	0.61	0.91	0.88	0.84	0.23	0.25	0.22

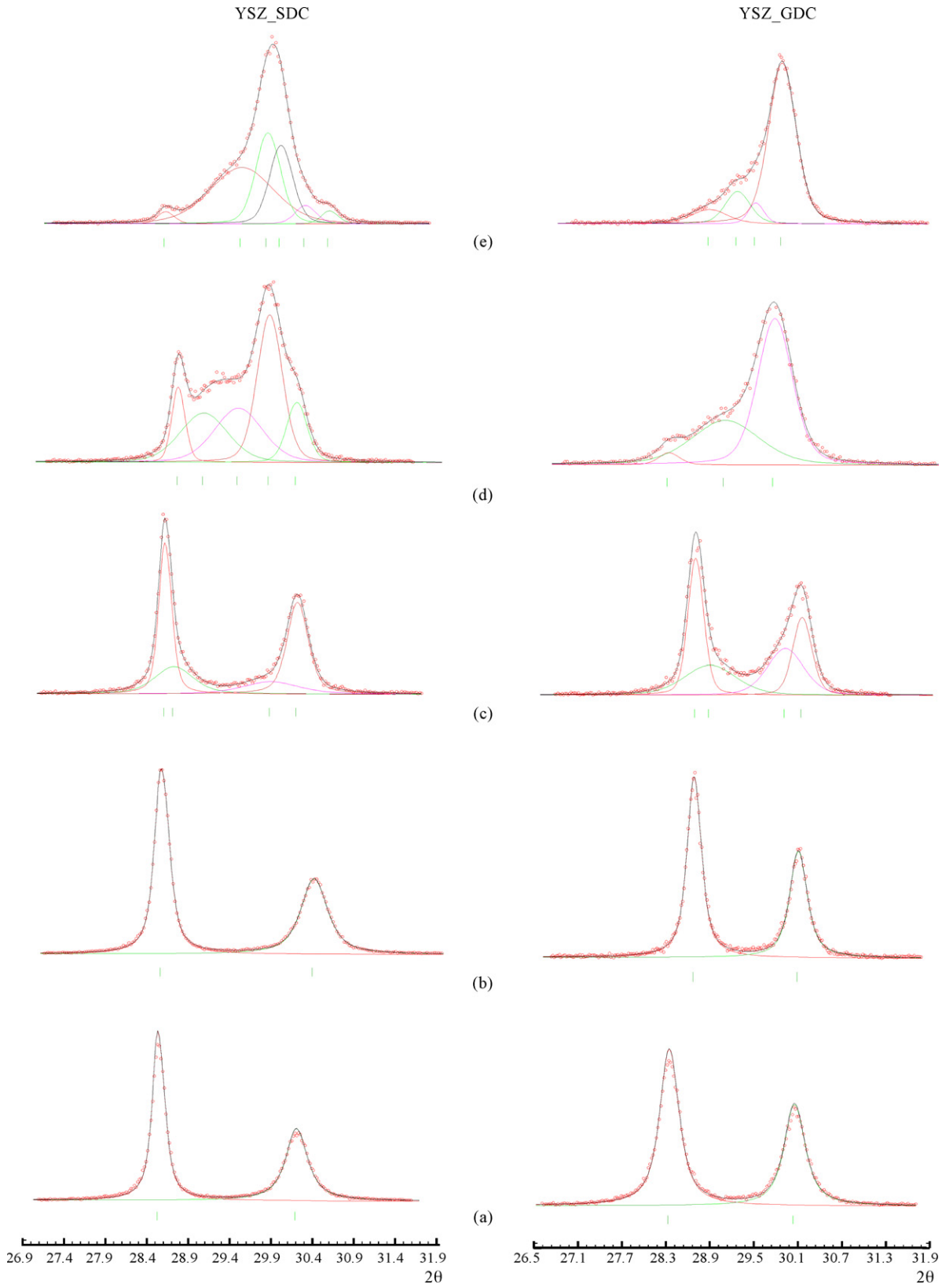

Fig. 8. Deconvolution of the first two peaks of the ceria–YSZ mixtures without structural model.

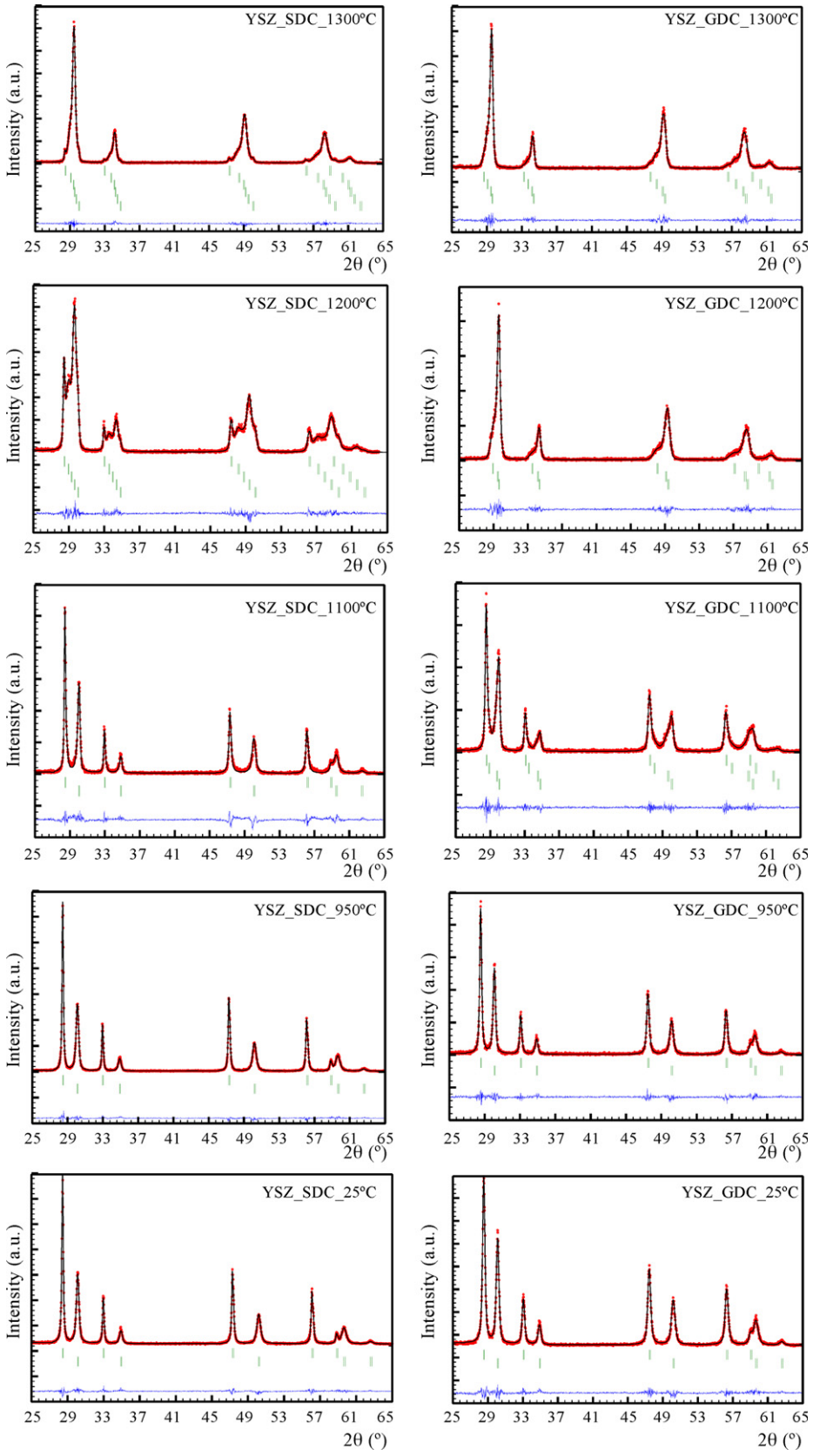

Fig. 9. Observed, calculated and difference X-ray powder diffraction patterns for electrolyte mixed with interlayer materials sintered at different temperatures.

Table 4
Proportion of YSZ–ceria materials in the different solid solution formed due the reaction between them

Mixture	Temperature (°C)				
	25	950	1100	1200	1300
SDC–YSZ	SDC YSZ	SDC YSZ	SDC $(SDC)_{0.95}(YSZ)_{0.05}$ $(SDC)_{0.65}(YSZ)_{0.35}$ YSZ	SDC $(SDC)_{0.95}(YSZ)_{0.05}$ $(SDC)_{0.58}(YSZ)_{0.42}$ $(SDC)_{0.35}(YSZ)_{0.65}$ YSZ	SDC $(SDC)_{0.71}(YSZ)_{0.29}$ $(SDC)_{0.59}(YSZ)_{0.41}$ $(SDC)_{0.45}(YSZ)_{0.55}$ $(SDC)_{0.34}(YSZ)_{0.66}$ YSZ
GDC–YSZ	GDC YSZ	GDC YSZ	$(GDC)_{0.73}(YSZ)_{0.27}$ $(GDC)_{0.67}(YSZ)_{0.33}$ $(GDC)_{0.59}(YSZ)_{0.41}$ $(GDC)_{0.10}(YSZ)_{0.90}$	$(GDC)_{0.62}(YSZ)_{0.38}$ $(GDC)_{0.53}(YSZ)_{0.47}$ $(GDC)_{0.41}(YSZ)_{0.59}$	$(GDC)_{0.62}(YSZ)_{0.38}$ $(GDC)_{0.52}(YSZ)_{0.48}$ $(GDC)_{0.47}(YSZ)_{0.53}$ $(GDC)_{0.46}(YSZ)_{0.54}$

Prof. First of all, the deconvolution of the initial two peaks of the X-ray diffraction measurements was considered. The numbers of presented phases in each diagram were evaluated using the peak-fit option of the WinPLOTR without structural model. The simulated profiles were then used to calculate the starting unit cell parameters from the 2θ position of the peaks (Fig. 8).

In the initial Rietveld analysis (structure profile refinement) the previously obtained unit cell parameters, peak shape (pseudo-Voigt), background, systematic 2θ shift, overall isotropic displacement, U, V, W half-width parameters for the profile function and asymmetry parameters were refined.

The fixed atomic coordinates for all the elements in the same cubic structure (SDC/GDC and YSZ) [11,16] permit the refinement of the occupation factors and the calculation of the weight percentage of the phases by modifying the ATZ parameter. The observed, calculated and difference X-ray powder diffraction patterns are shown in Fig. 9.

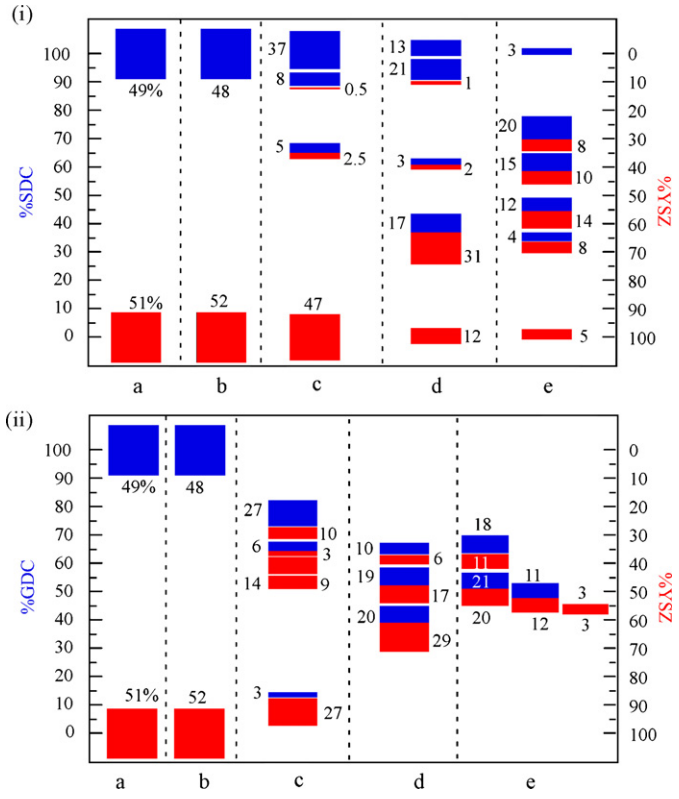

Fig. 10. Compositional gradient sequence in the reactivity between (i) YSZ-SDC and (ii) YSZ-GDC annealed at different temperature (a) 25 °C, (b) 950 °C, (c) 1100 °C, (d) 1200 °C and (e) 1300 °C. The squares represents the number of phases and the different colors the proportion of YSZ–ceria materials of each one. (For interpretation of the references to color in the figure caption, the reader is referred to the web version of the article.)

Therefore, the full-profile refinement allows in all cases to adjust the occupation factor for the Ce and Zr elements included initially as 50% in each compound. This procedure gives final occupation factor values for the elements showing a composition gradient, which is due to the substitution of Ce and Zr in the structures. The obtained quantitative phase analysis has been done taking into consideration the Brindley coefficient of microabsorption [19] for the mixtures treated at 25 and 950 °C. The grain growth by sintering processes at higher temperatures gives larger particle sizes, where the microabsorption effect was not significant. In all cases, the total fraction of ceria and zirconia in the presented compounds was in good agreement with the starting 50/50% weight mixtures.

The structural model refinement at different temperatures allows the calculation of the number of different compositions and the exact proportion of the YSZ and/or (SDC/GDC) in each one shown in Fig. 10 and Table 4. The change of the lattice parameter, grain size, crystal strain, grain boundary, stress and crystal distortion give rise to a variation of 2% in the obtained results.

The consecutive substitution of zirconia and ceria in the intermediate structures can play an important role in the resistance properties in the interlayer/electrolyte interface giving rise to mixtures with lower ionic conductivity than YSZ and/or (SDC/GDC) [20–22].

4. Conclusions

The ceria-based compounds as protective barriers play very significant role in the electrochemical behavior of the cathode part of SOFC performance. As already demonstrated in pervious investigations, the power density is increased probably on one hand, because the oxygen surface exchange kinetics of ceria is better than of zirconia's, and on the other hand, because the resistivity of the system is reduced when the ceria layer acts as a reaction barrier and prevents the formation of poorly conducting phases. However, one potential reason for this improvement is the formation of new intermediate compounds in the electrolyte/interlayer reaction frontier giving rise to a gradient composition sequence with high structural compatibility. The described three simultaneous processes could explain the significantly improved performance of the power densities with the incorporation of a Sm or Gd-doped CeO_2 layer between the Sr-doped lanthanum ferrite cathode and YSZ electrolyte in SOFCs.

Acknowledgements

This work has been financially supported by the "Departamento de Industria del Gobierno Vasco/Eusko Jaurlaritza", within

the strategic actions in Microenergy (GARAZI project, ETORTEK 2007-2009, SAIOTEK 2007 programmes). The authors thank the technicians of SGIker, financed by the "National Program for the Promotion of Human Resources within the National Plan of Scientific Research, Development and Innovation—"Ministerio de Ciencia y Tecnología", "Fondo Social Europeo (FSE)" and "Gobierno Vasco/Eusko Jaurlaritza, Dirección de Política Científica" for the X-ray diffraction measurements. A. Martínez-Amesti wishes to thank the "Gobierno Vasco/Eusko Jaurlaritza, Dirección de Política Científica" and UPV/EHU for funding.

References

[1] S.P. Simner, J.P. Shelton, M.D. Anderson, J.W. Stevenson, Solid States Ionics 161 (2003) 11.
[2] S.P. Simner, J.F. Bonnett, N.L. Canfield, K.D. Meinhardt, J.P. Shelton, V.L. Sprenkle, J.W. Stevenson, J. Power Sources 113 (2003) 1.
[3] S. Simner, M. Anderson, J. Bonnett, J. Stevenson, Solid State Ionics 175 (2004) 79.
[4] M.D. Anderson, J.W. Stevenson, S.P. Simner, J. Power Sources 129 (2004) 188.
[5] A. Mai, V.A.C. Haanappel, F. Tietz, D. Stöver, Solid State Ionics 177 (2006) 19.
[6] H.M. Rietveld, J. Appl. Crystallogr. 2 (1969) 65.
[7] J. Rodríguez-Carvajal, Phys. B 192 (1993) 55.
[8] J. Rodríguez-Carvajal, Fullprof, Rietveld Pattern Matching Analysis of Powder Patterns, 1994.
[9] S. Brunauer, P.H. Emmett, E. Teller, J. Am. Chem. Soc. 60 (1938) 309.
[10] S.E. Dann, D.B. Currie, M.T. Weller, M.F. Thomas, A.D. Al Rawwas, J. Solid State Chem. 109 (1994) 134.
[11] M. Yashima, S. Sasaki, M. Kakihana, Y. Yamaguchi, H. Arashi, M. Yoshimura, Acta Crystallogr., Sec. B 50 (1994) 663.
[12] M. Ahtee, Acta Crystallogr., Sec. B 34 (1978) 752.
[13] V. Adelskold, A. Kemie, Miner. Geol. 12A (1938) 1.
[14] J. Ten Elshof, J. Boeijsma, Powder Diffr. 11 (1996) 240.
[15] R.E. Hann, P.R. Suitch, J.L. Pentecost, J. Am. Ceram. Soc. 68 (1985) 285.
[16] G. Brauer, H. Gradinger, Z. Anorg. Allg. Chem. 276 (1954) 209.
[17] Inorganic Crystal Structure Database, ICSD for WWW, Fachin Formations Zentrum, Karlsruhe, Alemania, 2004.
[18] R.D. Shannon, Acta Crystallogr., Sec. A 32 (1976) 751.
[19] G.W. Brindley, Phil. Mag. 36 (1945) 347.
[20] G.Ch. Kostogloudis, G. Tsiniarakis, Ch. Ftikos, Solid States Ionics 135 (2000) 529.
[21] A. Tsoga, A. Gupta, A. Naoumidis, P. Nikolopoulos, Acta Mater. 48 (2000) 4709.
[22] X.-D. Zhou, B. Scarfino, H.U. Anderson, Solid State Ionics 175 (2004) 19.